

# Effects of rotation and anisotropy on the properties of type-II holographic superconductors

---

Jhony A. Herrera-Mendoza,<sup>a</sup> Alfredo Herrera-Aguilar,<sup>a</sup> Daniel F. Higuera-Borja,<sup>a,b</sup>  
Julio A. Méndez-Zavaleta,<sup>c</sup> Felipe Pérez-Rodríguez,<sup>a</sup> Jia-Xin Yin<sup>d</sup>

<sup>a</sup>*Instituto de Física, Benemérita Universidad Autónoma de Puebla, Edificio IF-1, Ciudad Universitaria, Puebla, Pue. 72570, México.*

<sup>b</sup>*Instituto de Física, Universidad de Antioquia, Calle 70 No 52-21, Medellín, Colombia.*

<sup>c</sup>*Facultad de Física, Universidad Veracruzana, Paseo No. 112, Desarrollo Habitacional Nuevo Xalapa, CP 91097, Xalapa-Enríquez, México.*

<sup>d</sup>*Department of Physics, Southern University of Science and Technology, Shenzhen, Guangdong 518055, China.*

*E-mail:* [jherrera@ifuap.buap.mx](mailto:jherrera@ifuap.buap.mx), [aherrera@ifuap.buap.mx](mailto:aherrera@ifuap.buap.mx),  
[dfhiguit@gmail.com](mailto:dfhiguit@gmail.com), [julmendez@uv.mx](mailto:julmendez@uv.mx), [fperez@ifuap.buap.mx](mailto:fperez@ifuap.buap.mx),  
[yinjx@sustech.edu.cn](mailto:yinjx@sustech.edu.cn)

**ABSTRACT:** The present work concerns the detailed construction of a holographic model for a type-II s-wave superconductor defined on a 5-dimensional anisotropic rotating black hole. We examine the role of rotation and anisotropy on the properties of the superconductor model focusing on the condensate and the AC conductivity, for which we obtain closed formulas, using both analytical and numerical methods. The results reveal that the rotation is responsible for the appearance of a peak and for introducing an exponentially vanishing behavior in the high-frequency limit of the real component of the AC conductivity. Such a behavior aligns with that observed in high-temperature superconductor models and experiments, where the peak and vanishing behavior result from quasiparticle damping, suggesting a plausible relation between the rotation of a black hole and quasiparticle damping effects in a superconducting material. In addition, we provide a detailed construction of the vortex lattice presented in [1] and study its behavior as a function of an external uniform magnetic field. Once again, it is shown that the vortex lattice can be continuously deformed along with a change in the vortex population by virtue of the magnetic field, providing a promising avenue for holographically modeling the vortex lattice deformations observed in experimental superconducting materials. As an observed experimental effect, we describe both the vortex lattice deformation and the vortex population increment under the action of an external magnetic field in the LiFeAs type-II superconductor. These effects supplement those previously found for the FeSe type-II superconductor studied in [1].

---

## Contents

<b>1</b>	<b>Introduction</b>	<b>1</b>
<b>2</b>	<b>The setup</b>	<b>2</b>
2.1	The decoupling limit	3
<b>3</b>	<b>Condensation of the scalar field</b>	<b>4</b>
<b>4</b>	<b>The AC conductivity</b>	<b>8</b>
4.1	Case $\Delta = 1$ and $z = 1$	9
4.2	Case $\Delta = 1$ and $z = 2$	11
<b>5</b>	<b>Turning on a uniform external magnetic field</b>	<b>13</b>
5.1	The external magnetic field	15
5.2	The vortex configuration	17
<b>6</b>	<b>Conclusions and discussion</b>	<b>20</b>

---

## 1 Introduction

Over the past years, the gauge/gravity duality has emerged as a powerful tool for investigating various phenomena within diverse physical contexts. Originally known as the AdS/CFT correspondence [2], it establishes a bridge between the behavior of a quantum field theory defined on a flat spacetime and the dynamics of a gravitational theory in a higher-dimensional spacetime. This approach has been particularly useful in studying the properties of strongly coupled quantum systems, such as those found in condensed matter physics and nuclear physics, where traditional analytical techniques fail to provide insight. In this regard, interesting explorations were given in condensed matter physics with a holographic description of field theory superconductors [3] and superfluids [4].

These seminal works laid the groundwork for future investigations within holographic superconductivity and superfluidity frameworks. A crucial fact is that holographic superconductors and superfluids can arise in a wide range of gravitational contexts supported by diverse matter fields. This includes gravitational backgrounds whose asymptotic is not only AdS but Lifshitz [5–10], which have proven useful to explore field theory systems with quantum critical regions governed by non-relativistic anisotropic scalings between space and time [11].

Concretely, holographic models for superconductors and superfluids have been extensively explored using asymptotically AdS backgrounds [3, 4, 12–15], including effects of

adding a uniform external magnetic field that led to the development of a holographic description of an Abrikosov vortex lattice[16–24]. On the other hand, holographic superconductors defined on non-relativistic backgrounds have been approached using asymptotically Lifshitz spacetimes [25–28]. Interestingly, and relevant to our present work, the effects of rotation have also been explored in scenarios with AdS [29–31] and Lifshitz asymptotic [1].

This work aims to develop a detailed and more comprehensive holographic model for a type-II superconductor that is defined on a rotating and anisotropic black hole configuration. By incorporating a rotating background, our primary goal is to investigate the impact of rotation on the properties of a holographic superconductor, with special attention to the condensate phenomena and AC conductivity for which closed expressions were obtained. The results suggest a relationship between the rotation of the black hole and quasiparticle damping effects induced by impurities or defects in a superconducting material. Additionally, we explore the formation of the vortex lattice and its deformation under an external magnetic field, a common feature of type-II superconductors. It is observed how infinitesimal variations of an external magnetic field influence the dynamics of vortices, changing their population and causing continuous deformations in the vortex lattice of type-II holographic superconductors.

*The manuscript is organized as follows:* in Sec. II we introduce the holographic setup working in the so-called probe limit. Sec. III is devoted to studying the condensation of the scalar field using both analytical and numerical methods, while Sec. IV presents an analytical treatment of the AC conductivity supplemented with numerical computations. In addition, in Sec. V we investigate the effect of a uniform external magnetic field on the vortex lattice, uncovering how the field influences the arrangement of vortices. We end in Sec. VI with a discussion and conclusions relevant to our findings.

## 2 The setup

According to the gauge/gravity correspondence, we start by defining the higher dimensional gravity theory of interest. For our purposes let us consider the following action

$$S = \int d^{d+2}x \sqrt{-g} \left( \mathcal{L}_{\text{bg}} - \frac{1}{q^2} \mathcal{L}_{\text{matter}} \right), \quad (2.1)$$

with background ( $\mathcal{L}_{\text{bg}}$ ) and matter ( $\mathcal{L}_{\text{matter}}$ ) Lagrangians given by

$$\mathcal{L}_{\text{bg}} = \frac{R - 2\lambda}{2\kappa} - \frac{1}{2} \nabla_\mu \varphi \nabla^\mu \varphi - \frac{1}{4} e^{-b\varphi} \mathcal{F}_{\mu\nu} \mathcal{F}^{\mu\nu}, \quad (2.2a)$$

$$\mathcal{L}_{\text{matter}} = \frac{1}{4} F_{\mu\nu} F^{\mu\nu} + \frac{1}{\ell^2} (|D_\mu \Psi|^2 + m^2 |\Psi|^2). \quad (2.2b)$$

The background Lagrangian  $\mathcal{L}_{\text{bg}}$  is defined by the Einstein-Hilbert action with cosmological constant  $\lambda$ , supplemented by a scalar dilaton field  $\varphi$  and a gauge field strength  $\mathcal{F}_{\mu\nu}$ . Moreover, the matter Lagrangian  $\mathcal{L}_{\text{matter}}$  is defined by a gauge field strength  $F_{\mu\nu}$  and a complex scalar field  $\Psi$ , charged by the covariant derivative  $D_\mu \equiv \nabla_\mu - iA_\mu$ . In addition, we take the limit  $q \rightarrow \infty$  wherein the Lagrangian  $\mathcal{L}_{\text{bg}}$  can be considered decoupled from  $\mathcal{L}_{\text{matter}}$ , such

that we can neglect the backreaction of  $\mathcal{L}_{\text{matter}}$  and work the equations of motion associated to  $\mathcal{L}_{\text{bg}}$  in order to look for a concrete gravitational solution with a manifest Lifshitz symmetry. Recall the rotating black hole solution for the  $\mathcal{L}_{\text{bg}}$  sector obtained in [32]

$$ds^2 = -\left(\frac{r}{\ell}\right)^{2z} f(r) \left( \Xi dt - \sum_{i=1}^n a_i d\phi_i \right)^2 + \frac{r^2}{\ell^4} \sum_{i=1}^n (a_i dt - \Xi \ell^2 d\phi_i)^2 + \frac{dr^2}{\left(\frac{r}{\ell}\right)^2 f(r)} - \frac{r^2}{\ell^2} \sum_{i<j}^n (a_i d\phi_j - a_j d\phi_i)^2 + \left(\frac{r}{\ell}\right)^2 d\vec{y}_{(d-n)}^2, \quad (2.3)$$

with

$$\begin{aligned} f(r) &= 1 - \left(\frac{r_h}{r}\right)^{z+d}, & e^{-b\varphi} &= \kappa \frac{Q^2 \ell^2}{(z-1)(z+d)} \left(\frac{\ell}{r}\right)^{2d}, \\ \mathcal{F}_{tr} &= \Xi \frac{(z-1)(z+d)}{\kappa Q \ell^2} \left(\frac{r}{\ell}\right)^{d+z-1}, & \mathcal{F}_{\phi_i r} &= -a_i \frac{(z-1)(z+d)}{\kappa Q \ell^2} \left(\frac{r}{\ell}\right)^{d+z-1}, \\ \Lambda &= -\frac{(z+d)(z+d-1)}{2\ell^2}, & b &= 2\sqrt{\frac{\kappa d}{z-1}}, \end{aligned} \quad (2.4)$$

where  $n = [(d+1)/2]$  is the maximal number of independent rotation planes possible in  $d+2$  dimensions, each plane having associated a rotation parameter  $a_i$ , while  $\Xi = \sqrt{1 + \sum_{i=1}^n a_i^2/\ell^2}$ , and  $d\vec{y}_{(d-n)}^2 = dy_k dy^k$  is the Euclidean metric in  $d-n$  dimensions. We take the particular case of 5 dimensions and assume only one non-trivial rotation parameter ( $a_1 = a$  and  $a_2 = 0$ ). In this case, the metric is reduced to

$$ds^2 = -\left(\frac{r}{\ell}\right)^{2z} f(r) (\Xi dt - a d\phi)^2 + \frac{r^2}{\ell^4} (adt - \Xi \ell^2 d\phi)^2 + \frac{dr^2}{\left(\frac{r}{\ell}\right)^2 f(r)} + \left(\frac{r}{\ell}\right)^2 d\vec{y}^2, \quad (2.5)$$

with  $d\vec{x}^2 = dx^2 + dy^2$  and  $f(r) = 1 - \left(\frac{r_h}{r}\right)^{z+3}$ .

## 2.1 The decoupling limit

As we discussed before, in the limit  $q \rightarrow \infty$ , the feedback or backreaction of the matter fields in  $\mathcal{L}_{\text{matter}}$  is suppressed on the bulk fields of  $\mathcal{L}_{\text{bg}}$ . In this manner, we obtain the following set of field equations on the now fixed background (2.5), i.e.

$$\nabla_\mu F^{\mu\nu} - \frac{1}{\ell^2} (2A^\nu |\Psi|^2 - i\Psi \nabla^\nu \bar{\Psi} + i\bar{\Psi} \nabla^\nu \Psi) = 0, \quad (2.6a)$$

$$\nabla^\mu \nabla_\mu \Psi - 2iA^\mu \nabla_\mu \Psi - i\Psi \nabla_\mu A^\mu - (m^2 + A_\mu A^\mu) \Psi = 0. \quad (2.6b)$$

Next, we take the most general stationary and axisymmetric ansätze for the matter fields compatible with the metric structure (2.5),

$$\Psi = \Psi(r, \vec{y}), \quad A_t = A_t(r, \vec{y}), \quad A_\phi = A_\phi(r, \vec{y}), \quad A_x = A_x(r, \vec{y}), \quad A_y = A_y(r, \vec{y}). \quad (2.7)$$

For simplicity, we redefine the holographic coordinate as  $u = r_h/r$ , in which the boundary and horizon are located at  $u = 0$  and  $u = 1$ , respectively. By taking into account the

previous information, the field equations (2.6) reduce to the following coupled nonlinear system of partial differential equations.

The scalar equation

$$\begin{aligned} \partial_{uu}^2 \Psi + \left[ \frac{\partial_u f}{f} - \frac{(z+2)}{u} \right] \partial_u \Psi + \frac{\ell^4}{r_h^2 f} (\partial_{xx}^2 + \partial_{yy}^2) \Psi - \frac{i\ell^4}{r_h^2 f} [(\partial_x A_x + \partial_y A_y) \Psi + 2A_x \partial_x \Psi \\ + 2A_y \partial_y \Psi] - \left\{ \frac{\ell^2}{u^2 f} \left[ m^2 + (\ell^2(A_x^2 + A_y^2) + (aA_t + \Xi A_\phi)^2) \left( \frac{u}{r_h} \right)^2 \right] \right. \\ \left. - \left( \frac{\ell u}{r_h} \right)^{2(z-1)} \frac{(\ell^2 \Xi A_t + aA_\phi)^2}{r_h^2 f^2} \right\} \Psi = 0, \end{aligned} \quad (2.8)$$

and the Maxwell equations

$$\begin{aligned} \partial_{uu}^2 A_t + \left[ \frac{2a^2(z-1) + \ell^2(z-2)}{u} - a^2 \frac{\partial_u f}{f} \right] \frac{\partial_u A_t}{\ell^2} + \left[ \frac{2a\Xi(z-1)}{u} - a\Xi \frac{\partial_u f}{f} \right] \frac{\partial_u A_\phi}{\ell^2} \\ + \frac{\ell^4}{r_h^2 f} (\partial_{xx}^2 + \partial_{yy}^2) A_t - \frac{2}{u^2 f} |\Psi|^2 A_t = 0, \end{aligned} \quad (2.9a)$$

$$\begin{aligned} \partial_{uu}^2 A_\phi - \left[ \frac{2a^2(z-1) + \ell^2 z}{u} - \ell^2 \Xi^2 \frac{\partial_u f}{f} \right] \frac{\partial_u A_\phi}{\ell^2} - \left[ \frac{2a\Xi(z-1)}{u} - a\Xi \frac{\partial_u f}{f} \right] \partial_u A_t \\ + \frac{\ell^4}{r_h^2 f} (\partial_{xx}^2 + \partial_{yy}^2) A_\phi - \frac{2}{u^2 f} |\Psi|^2 A_\phi = 0, \end{aligned} \quad (2.9b)$$

$$\begin{aligned} \partial_{uu}^2 A_y + \left( \frac{\partial_u f}{f} - \frac{z}{u} \right) \partial_u A_y + \frac{\ell^4}{r_h^2 f} (\partial_{xx}^2 A_y - \partial_{xy}^2 A_x) + \frac{2}{u^2 f} \Im(\bar{\Psi} \partial_y \Psi) \\ - \frac{2}{u^2 f} |\Psi|^2 A_y = 0, \end{aligned} \quad (2.9c)$$

$$\begin{aligned} \partial_{uu}^2 A_x + \left( \frac{\partial_u f}{f} - \frac{z}{u} \right) \partial_u A_x + \frac{\ell^4}{r_h^2 f} (\partial_{yy}^2 A_x - \partial_{xy}^2 A_y) + \frac{2}{u^2 f} \Im(\bar{\Psi} \partial_x \Psi) \\ - \frac{2}{u^2 f} |\Psi|^2 A_x = 0, \end{aligned} \quad (2.9d)$$

$$\partial_{ux}^2 A_x + \partial_{uy}^2 A_y - \frac{r_h^2}{\ell^4 u^2} 2\Im(\bar{\Psi} \partial_u \Psi) = 0, \quad (2.9e)$$

We notice a strong coupling between the vector and scalar sectors, even when disregarding the background interaction. While finding an exact solution remains unattainable, the subsequent section delves into an approach that facilitates the characterization of the physics associated with these fields.

### 3 Condensation of the scalar field

We know that superconductors are characterized by the presence of a scalar field acting as the order parameter that condensates at some critical temperature. Here, we want to explore whether the scalar field  $\Psi$  possesses such a property. To do so, it is sufficient to consider real scalar and gauge fields with the simplest ansätze consistent with the equations (2.8) and (2.9), i.e.

$$\Psi = \psi(u), \quad A_t = A_t(u), \quad A_\phi = A_\phi(u), \quad A_x = 0, \quad A_y = 0. \quad (3.1)$$

In such a scenario the system of equations (2.8)-(2.9) reduces to

$$A_t'' + \left[ \frac{2a^2(z-1) + \ell^2(z-2)}{u} - a^2 \frac{f'}{f} \right] \frac{A_t'}{\ell^2} + \left[ \frac{2a\Xi(z-1)}{u} - a\Xi \frac{f'}{f} \right] \frac{A_\phi'}{\ell^2} - \frac{2}{u^2 f} \psi^2 A_t = 0, \quad (3.2a)$$

$$A_\phi'' - \left[ \frac{2a^2(z-1) + \ell^2 z}{u} - \ell^2 \Xi^2 \frac{f'}{f} \right] \frac{A_\phi'}{\ell^2} - \left[ \frac{2a\Xi(z-1)}{u} - a\Xi \frac{f'}{f} \right] A_t' - \frac{2}{u^2 f} \psi^2 A_\phi = 0, \quad (3.2b)$$

$$\psi'' + \left[ \frac{f'}{f} - \frac{(z+2)}{u} \right] \psi' - \left\{ \frac{\ell^2 (aA_t + \Xi A_\phi)^2}{r_h^2 f} - \left( \frac{\ell u}{r_h} \right)^{2(z-1)} \frac{(\ell^2 \Xi A_t + aA_\phi)^2}{r_h^2 f^2} + \frac{\ell^2 m^2}{u^2 f} \right\} \psi = 0 \quad (3.2c)$$

Now, we propose Taylor series expansions of the fields around the horizon  $u = 1$

$$\psi(u) = \psi(1) + \psi'(1)(u-1) + \frac{\psi''(1)}{2}(u-1)^2 + \dots \quad (3.3a)$$

$$A_t(u) = A_t(1) + A_t'(1)(u-1) + \frac{A_t''(1)}{2}(u-1)^2 + \dots \quad (3.3b)$$

$$A_\phi(u) = A_\phi(1) + A_\phi'(1)(u-1) + \frac{A_\phi''(1)}{2}(u-1)^2 + \dots \quad (3.3c)$$

Here, to have a regular gauge field at the horizon, we need the boundary conditions

$$A_t(1) = 0, \quad A_\phi(1) = 0, \quad (3.4)$$

while the boundary condition for  $\psi(1)$  is arbitrary but finite. The remaining coefficients are determined by making the expansions (3.3) consistent with the field equations (3.2). After some algebraic computations, we find

$$A_\phi'(1) = -\frac{a}{\Xi} A_t'(1), \quad \psi'(1) = -\frac{\ell^2 m^2}{z+3} \psi(1); \quad (3.5a)$$

$$A_t''(1) = -\frac{2\psi(1)^2 + (z+3)(z-2)}{z+3} A_t'(1), \quad A_\phi''(1) = -\frac{a}{\Xi} A_t''(1); \quad (3.5b)$$

$$\psi''(1) = \frac{\ell^2 m^2}{z+3} \left[ 1 + \frac{\ell^2 m^2}{2(z+3)} \right] \psi(1) - \frac{\ell^2 A_t'(1)^2}{2\Xi^2 (z+3)^2} \left( \frac{\ell}{r_h} \right)^{2z} \psi(1). \quad (3.5c)$$

Note that the higher-order terms are also expressed in terms of the lowest-order ones.

On the other hand, in order for the fields to have a correct interpretation from the holographic point of view, the near boundary ( $u \rightarrow 0$ ) behavior must have the form  $\psi \sim u^\Delta$ ,  $A_t \sim u^{\alpha_1}$  and  $A_\phi \sim u^{\alpha_2}$  with  $\Delta$ ,  $\alpha_1$  and  $\alpha_2$  non-negative numbers. After substitution into the field equation (3.2) and taking the limit  $u \rightarrow 0$  we are left with the regular solutions

$$\psi = J_- u^{\Delta_-} + J_+ u^{\Delta_+}, \quad A_t = \mu - \rho \left( \frac{u}{r_h} \right)^{3-z}, \quad A_\phi = \nu - \zeta \left( \frac{u}{r_h} \right)^{3-z}, \quad (3.6)$$

provided  $z \leq 3$ , where  $\Delta$  is interpreted as the scaling dimension of the dual scalar operator (order parameter)  $\mathcal{O}$ , which is found to be  $\Delta_{\pm} = [(z+3) \pm \sqrt{(z+3)^2 + 4\ell^2 m^2}]/2$ . Moreover,  $\mu$  and  $\nu$  are interpreted as potentials in the dual field theory, while  $\rho$  and  $\zeta$  are respectively the charge and the current density. For this specific field configuration, these densities are related to each other by  $\zeta = -\frac{a}{\Xi}\rho$ .<sup>1</sup> In addition, to keep the arguments as simple as possible we also impose the boundary condition  $J_- = 0$  and set  $J_+ = J$ ,  $\Delta_+ = \Delta$ , i.e., we are considering  $J_+$  as the expectation value of the order parameter with scaling dimension  $\Delta$ , and  $J_-$  as its source.

Thus far we have found expressions for both regimes, near horizon ( $u = 1$ ) and asymptotic ( $u = 0$ ) solutions. In what follows, we impose the fundamental requirement that there is an intermediate point  $u = u_m$  in the bulk where the asymptotic solutions, (3.6) and (3.3), match and their first derivatives as well. This assumption leads us to four independent relations

$$J u_m^{\Delta} = \psi(1) - \frac{\ell^2 m^2}{z+3} \psi(1)(u_m - 1) + \left\{ \frac{\ell^2 m^2}{z+3} \left[ 1 + \frac{\ell^2 m^2}{2(z+3)} \right] - \frac{\ell^2 A'_t(1)^2}{2\Xi^2(z+3)^2} \left( \frac{\ell}{r_h} \right)^{2z} \right\} \frac{\psi(1)}{2} (u_m - 1)^2, \quad (3.7a)$$

$$J \Delta u_m^{\Delta-1} = -\frac{\ell^2 m^2}{z+3} \psi(1) + \left\{ \frac{\ell^2 m^2}{z+3} \left[ 1 + \frac{\ell^2 m^2}{2(z+3)} \right] - \frac{\ell^2 A'_t(1)^2}{2\Xi^2(z+3)^2} \left( \frac{\ell}{r_h} \right)^{2z} \right\} \psi(1)(u_m - 1), \quad (3.7b)$$

$$\mu - \rho \left( \frac{u_m}{r_h} \right)^{3-z} = A'_t(1)(u_m - 1) - \frac{2\psi(1)^2 + (z+3)(z-2)}{2(z+3)} A'_t(1)(u_m - 1)^2, \quad (3.7c)$$

$$-(3-z) \frac{\rho}{r_h} \left( \frac{u_m}{r_h} \right)^{2-z} = A'_t(1) - \frac{2\psi(1)^2 + (z+3)(z-2)}{z+3} A'_t(1)(u_m - 1). \quad (3.7d)$$

From (3.7a) and (3.7b) we arrive at

$$J = \frac{u_m^{1-\Delta} [\ell^2 m^2 (1-u_m) + 2(z+3)]}{(z+3) [\Delta(1-u_m) + 2u_m]} \psi(1), \quad (3.8a)$$

$$A'_t(1) = -\gamma \Xi \left( \frac{r_h}{\ell} \right)^z, \quad (3.8b)$$

where

$$\gamma = \sqrt{\ell^2 m^4 + \frac{2\ell^2 m^2 (z+3) \{u_m [u_m (\Delta-2) - 4(\Delta-1)] + 3\Delta\} + 4\Delta (z+3)^2}{\ell^2 [\Delta(1-u_m) + 2u_m] (1-u_m)}}. \quad (3.9)$$

Similarly, from (3.7d) we obtain

$$\psi(1)^2 = \frac{(z+3)}{2(1-u_m)} \left[ \frac{\ell^z (3-z)}{\gamma \Xi r_h^3} \rho u_m^{2-z} - (z-2)(1-u_m) - 1 \right]. \quad (3.10)$$

---

<sup>1</sup>Note that there is another branch of solutions,  $\alpha_1 = \alpha_2 = z+1$  with  $\zeta = -\frac{\Xi \ell^2}{a} \rho$ . Nevertheless, they are inconsistent with the upcoming procedure and will be discarded.

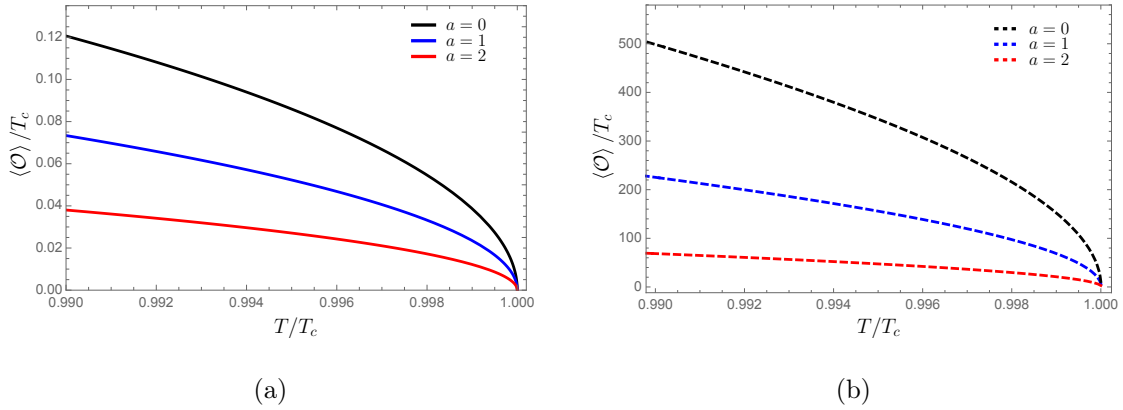


**Figure 1:** The condensation operator for different values of the rotation parameter. Figure (a) portrays the condensation of the dual operator derived through the matching method as shown in equation (3.14) when  $u_m = 0.8$ ,  $z = 2$ , and  $\ell^2 m^2 = -3$ . On the other hand, Figure (b) presents the results obtained by numerically solving the system (3.2) using the shooting method with  $z = 2$  and  $\ell^2 m^2 = -3$ .

At this point let us recall the temperature of the black hole (2.5), which has the form [32]

$$T = \frac{1}{4\pi} \frac{(z+3)r_h^z}{\ell^{z+1}\Xi}, \quad (3.11)$$

allowing us to write (3.10) as an explicit function of the black hole temperature

$$\psi(1)^2 = \frac{(z+3)}{2(1-u_m)} \left[ \frac{\ell^z(3-z)}{\gamma\Xi^{1+3/z}} \left( \frac{z+3}{4\pi\ell^{z+1}} \right)^{3/z} \frac{\rho u_m^{2-z}}{T^{3/z}} - (z-2)(1-u_m) - 1 \right]. \quad (3.12)$$

The holographic dictionary facilitates a connection between the expectation value of the dual operator  $\langle \mathcal{O} \rangle$  and the coefficient associated with the subleading order of the scalar field  $J$ . Concretely we get,  $\langle \mathcal{O} \rangle = \sqrt{2}r_h^\Delta J$ , where the critical temperature is reached when  $\langle \mathcal{O} \rangle = 0$ , or equivalently  $\psi(1) = 0$ . Thus we arrive at the critical temperature for the condensation to occur

$$T_c = \frac{\ell^{z(z-3)/3-1}(z+3)}{4\pi\Xi^{1+z/3}} \left\{ \frac{(3-z)\rho u_m^{2-z}}{\gamma[(z-2)(1-u_m)+1]} \right\}^{z/3}. \quad (3.13)$$

Therefore, the expectation value for the condensation operator reads

$$\langle \mathcal{O} \rangle = \left( \frac{4\pi\ell^{z+1}\Xi T_c}{z+3} \right)^{\Delta/z} \left( \frac{T}{T_c} \right)^{(2\Delta-3)/2z} \frac{u_m^{1-\Delta} [\ell^2 m^2 (1-u_m) + 2(z+3)]}{\Delta(1-u_m) + 2u_m} \times \sqrt{\frac{1+(z-2)(1-u_m)}{(z+3)(1-u_m)} \left[ 1 - \left( \frac{T}{T_c} \right)^{3/z} \right]}. \quad (3.14)$$

From this, we identify different behaviors depending on the sign of the power  $2\Delta - 3$ . Nevertheless, near the critical point  $T = T_c$ , the behavior is the same for any of the cases.



Figure 1 depicts the condensation of the dual operator  $\langle \mathcal{O} \rangle$  from two different perspectives: analytical (matching method) and numerical (shooting method). While both methods measure the same quantity, there are significant variations between them, as observed in the plots. However, it is not surprising that they do not yield identical results. Recall that the matching method involves an additional parameter,  $u_m$ , whose selection strongly influences the results for  $\langle \mathcal{O} \rangle$ . Hence, it only offers a qualitative explanation of the phenomenon. In contrast, the shooting method provides a more accurate depiction as it does not introduce any additional parameters and aligns with the anticipated outcome of the matching method. In other words, both figures exhibit the impact of varying the rotation parameter, which only decreases the amplitude of the expectation value for the condensation operator when increasing the rotation.

#### 4 The AC conductivity

The AC conductivity is an important quantity characterizing a field theory superconductor as the response of the system to electric perturbations. In our holographic setup, this can be studied by introducing a gauge field perturbation within the bulk dynamics and working the linearized Maxwell equations. Hence, considering the bulk perturbation along the  $x$  component of the gauge field and assuming a time dependence of the form  $\delta A_x = A_x(u)e^{-i\omega t}$ , from (2.6) we arrive at the following equation

$$A_x'' + \left( \frac{f'}{f} - \frac{z}{u} \right) A_x' + \left[ \left( \frac{\ell u}{r_h} \right)^{2z} \frac{\omega^2 \ell^2 \Xi^2}{f} - \left( \frac{\ell^2 a^2 \omega^2 u^2}{r_h^2} + 2\psi^2 \right) \right] \frac{A_x}{u^2 f} = 0. \quad (4.1)$$

We solve this equation by imposing an ingoing wave condition at the horizon

$$A_x = (u-1)^{-i \frac{\ell^{z+1}}{(z+3)r_h^z} \omega} \left[ 1 + A_{x1}(u-1) + A_{x2}(u-1)^2 + \dots \right], \quad (4.2)$$

while the asymptotic behavior at the boundary has the form

$$A_x = A_x^{(0)} + A_x^{(z+1)} \left( \frac{u}{r_h} \right)^{z+1} + \dots, \quad (4.3)$$

where the standard holographic dictionary allows  $A_x^{(0)}$  to be interpreted as the source of a conjugated current  $J_x$ , while  $A_x^{(z+1)}$  corresponds to its expectation value,  $\langle J_x \rangle \propto A_x^{(z+1)}$ . In this sense, from the Ohm law, we obtain an expression for the AC conductivity

$$\sigma(\omega) = \frac{\langle J_x \rangle}{E_x} = - \frac{(z+1)i}{\omega} \frac{A_x^{(z+1)}}{A_x^{(0)}}. \quad (4.4)$$

In the remainder of this section, we are interested in investigating the frequency and angular momentum dependence of the conductivity. For this purpose, we conduct an analytical study of the Maxwell perturbation (4.1) by focussing on the near-boundary limit of the anisotropic background. This is achieved by considering  $f \approx 1$  and  $\psi \approx \langle \mathcal{O} \rangle u^\Delta / \sqrt{2}$ , yielding

$$A_x'' - \frac{z}{u} A_x' + \left[ \left( \left( \frac{\ell u}{r_h} \right)^{2z} \frac{\ell^2 \Xi^2}{u^2} - \frac{\ell^2 a^2}{r_h^2} \right) \omega^2 - \frac{2 \langle \mathcal{O} \rangle^2}{r_h^2} \left( \frac{u}{r_h} \right)^{2(\Delta-1)} \right] A_x = 0. \quad (4.5)$$

The analytical solutions of this equation are only possible when considering particular values of the parameters  $\Delta$  and  $z$ . In the subsequent pages, we illustrate some examples in which this can be done. In addition, we supplement our analytical computations with numerical ones by solving the full equation (4.1) subject to the boundary conditions (4.2) and (4.3).

#### 4.1 Case $\Delta = 1$ and $z = 1$

In this case, the equation (4.5) has two independent solutions that can be expressed in terms of the Bessel functions of the first  $J_1$  and second kind  $Y_1$

$$A_x(u) = c_0 u J_1(i h(\omega) u) + c_1 u Y_1(-i h(\omega) u), \quad (4.6)$$

with

$$h(\omega) \equiv \frac{\sqrt{\langle \mathcal{O} \rangle^2 - \ell^4 \omega^2}}{r_h}. \quad (4.7)$$

Before proceeding, we find convenient the identification

$$\frac{c_0}{c_1} = \frac{i}{\pi} \left[ \pi H(\omega - \omega_g) + (1 - 2\gamma_E)i + \frac{2\omega}{h^2(\omega)} \left( \frac{950}{\omega} - 5 \right) + \frac{1}{100} i \ln \left( \frac{h^2(\omega)}{4} \right) - \frac{\pi}{2} \right], \quad (4.8)$$

wherein  $H(\omega - \omega_g)$  is the Heaviside step function and  $\gamma_E$  is the Euler constant. Thence, the asymptotic analysis of the solution (4.6), in conjunction with the relation (4.4), provides the following result for the conductivity

$$\sigma(\omega) = -\frac{h^2(\omega)}{200\omega} \left( 201\pi H(\omega - \omega_g) + 101 i \ln \left( \frac{h^2(\omega)}{4} \right) - 500 i \frac{\omega}{h^2(\omega)} \left( \frac{190}{\omega} - 1 \right) \right). \quad (4.9)$$

A closer inspection of this expression reveals the structure of real and imaginary parts of the conductivity, giving rise to

$$\text{Re}[\sigma] = \begin{cases} \infty & \omega = 0, \\ 0 & 0 < \omega \leq \omega_g, \\ -\frac{\pi h^2(\omega)}{2\omega} & \omega > \omega_g, \end{cases} \quad (4.10)$$

$$\text{Im}[\sigma] = \begin{cases} -\frac{101 h^2(\omega)}{200\omega} \ln \left( \frac{h^2(\omega)}{4} \right) + \frac{1}{2} \left( \frac{950}{\omega} - 5 \right) & 0 < \omega < \omega_g, \\ -\frac{101 h^2(\omega)}{200\omega} \ln \left( \frac{|h^2(\omega)|}{4} \right) + \frac{1}{2} \left( \frac{950}{\omega} - 5 \right) & \omega > \omega_g. \end{cases} \quad (4.11)$$

Here,  $\omega_g = \langle \mathcal{O} \rangle / \ell^2$  denotes a gap frequency determined by the function  $h(\omega)$  below which the real part of the conductivity drops to zero, except at  $\omega = 0$ , where a delta function appears.

In Figure 2, we show the behavior of the real and imaginary parts of the conductivity defined by these expressions. The observed behavior exhibits recurring characteristics found in previous holographic models for superconductors. Concerning the real part of the conductivity, the delta function at  $\omega = 0$  suggests the presence of a DC current and the

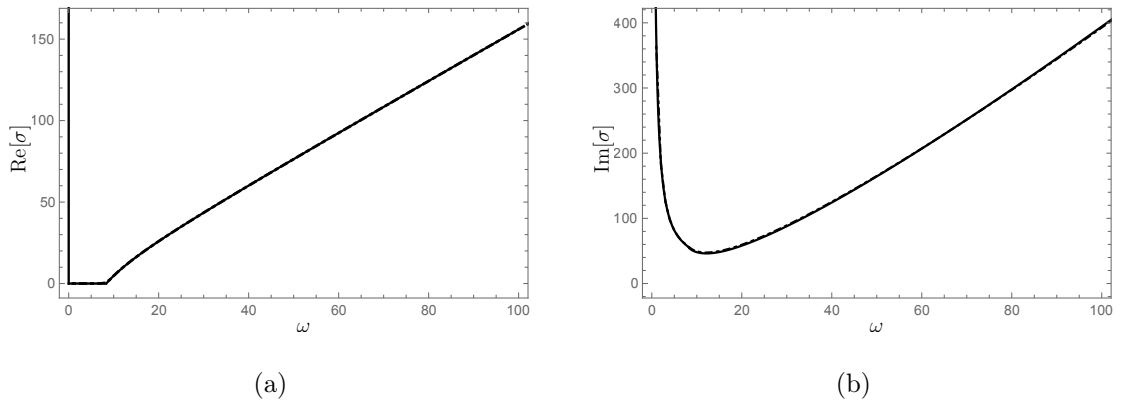


**Figure 2:** Sketches for the real (a) and imaginary (b) components of the conductivity as a function of the frequency. Note the excellent agreement between the analytical (solid lines) and the numerical results (dashed lines). These plots were generated at  $T \approx 0.93 T_c$  with  $\langle \mathcal{O} \rangle \approx 8.344$ , considering parameters  $\ell = 1$  and  $r_h = 1$ .

onset of the superconducting state. Moreover, the existence of a gap frequency  $\omega_g$ , which is proportional to the order parameter  $\langle \mathcal{O} \rangle$ , is also a common property in holographic superconductors. However, it has been argued that holographic superconductors are not gapped. Instead, the apparent gap is the result of decoupling the matter sector from the gravity, a consequence of employing the probe limit method. For an in-depth exploration of this matter, we refer the reader to [13, 33, 34]. For frequencies above the gap frequency  $\omega > \omega_g$ , the behavior is governed by the monotonic increasing function  $\text{Re}[\sigma] \sim -h^2(\omega)/\omega$ , following a linear tendency  $\text{Re}[\sigma] \sim \omega$  at sufficiently higher frequencies.

Turning our attention to the imaginary component, we observe the presence of a minimum occurring near  $\omega_g$ . Below this minimum, at lower frequencies, the abrupt increasing behavior is defined by  $\text{Im}[\sigma] \sim 1/\omega$ . On the other hand, at sufficiently higher frequencies  $\omega \gg \omega_g$ , the behavior is dictated by  $\text{Im}[\sigma] \sim \omega \ln(\ell^2 \omega / 2r_h)$ . All these behaviors are contained in Figure 2, where we highlight the remarkable consistency between our analytical predictions (solid lines) and the numerical computations (dashed lines).

Lastly, it is important to note that we have not addressed the rotation of the background in the previous scenario. The reason for this is that neither of the expressions, (4.10) or (4.11), possess information on the rotation parameter  $a$ . This observation results evident from the effective equation (4.5), where the absence of anisotropy ( $z = 1$ ) leads to the cancellation of terms associated with rotation, rendering no residual information on this parameter. Consequently, we infer that anisotropy ( $z \neq 1$ ) is an essential ingredient for discerning the impact of rotation on the AC conductivity, at least in the case that concerns our holographic model.

## 4.2 Case $\Delta = 1$ and $z = 2$

In this scenario, the solution can be written in terms of the confluent hypergeometric functions of the first kind,  $M$ , and the second kind,  $U$ ,

$$A_x(u) = e^{-i\frac{\ell^3 \Xi \omega}{2r_h^2} u^2} u^3 \left[ c_0 M \left( \frac{5}{4} - ig(\omega, a), \frac{5}{2}, i\frac{\Xi \ell^3 \omega}{r_h^2} u^2 \right) + c_1 U \left( \frac{5}{4} - ig(\omega, a), \frac{5}{2}, i\frac{\Xi \ell^3 \omega}{r_h^2} u^2 \right) \right], \quad (4.12)$$

where we define

$$g(\omega, a) \equiv \frac{1}{4\ell\Xi} \left( a^2 \omega + \frac{\langle \mathcal{O} \rangle^2}{\ell^2 \omega} \right). \quad (4.13)$$

As in the preceding case, we can obtain an analytic expression for the conductivity using the relation (4.4). To accomplish this, we find it convenient to make the identification

$$\frac{c_0}{c_1} = - \frac{\sqrt{\pi} e^{\pi g(\omega, a)} (1 - i e^{2\pi g(\omega, a)})}{(e^{4\pi g(\omega, a)} + 1) \Gamma(-\frac{1}{4} - ig(\omega, a))} \left( \mathcal{F}(a) e^{-\pi g(\omega, a)} + \frac{4}{3} i e^{\pi g(\omega, a)} + i \mathcal{G}(a, \omega) \left( \frac{r_h^2}{\ell^3 \Xi} \right)^{3/2} \frac{|\Gamma(-\frac{1}{4} + ig(\omega, a))|^2}{2\pi(z+1)\omega^{1/2} \operatorname{sech}(2\pi g(\omega, a))} \right), \quad (4.14)$$

in which the functions  $\mathcal{F}(a)$  and  $\mathcal{G}(a, \omega)$  adopt respectively the form

$$\mathcal{F}(a) = \frac{448}{5} \left( \frac{a}{\ell} \right)^6 - \frac{15147}{100} \left( \frac{a}{\ell} \right)^5 + \frac{11171}{100} \left( \frac{a}{\ell} \right)^4 - \frac{125}{4} \left( \frac{a}{\ell} \right)^3 + \frac{337}{100} \left( \frac{a}{\ell} \right)^2 - \frac{11}{250} \left( \frac{a}{\ell} \right) + \frac{1601}{600}, \quad (4.15a)$$

$$\mathcal{G}(a, \omega) = \ell \left[ 9543 \left( \frac{a}{\ell} \right)^2 - 3493 \left( \frac{a}{\ell} \right) + 379 + \left( 10^6 \left( \frac{a}{\ell} \right)^2 + 5 \right) \ell \omega + \frac{6 \times 10^7}{\ell \omega} \right]. \quad (4.15b)$$

Altogether, with the aid of the above definitions, we arrive at the following expression for the conductivity

$$\sigma(\omega) = 6\pi \left( \frac{\ell^3 \Xi}{r_h^2} \right)^{3/2} \omega^{1/2} \left( \mathcal{F}(a) - \frac{4}{3} \right) \frac{\operatorname{sech}(2\pi g(\omega, a))}{|\Gamma(-\frac{1}{4} + ig(\omega, a))|^2} e^{-\pi g(\omega, a)} + i \mathcal{G}(a, \omega). \quad (4.16)$$

In contrast with the previous case, the conductivity in this scenario contains an explicit dependency on the rotation parameter  $a$ . This makes reasonable the questioning of how the rotation influences the AC conductivity, as shown in Figure 3. To address this question, let us first examine the case devoid of rotation, where  $a = 0$ . This scenario is represented by the black curves in Figure 3. In this case, in conjunction with (4.16), the real part of the conductivity also has a delta function at  $\omega = 0$ . This arises from the behavior of the denominator  $|\Gamma(-\frac{1}{4} + ig(\omega, a))|^2$ , which goes to zero more rapidly than it does the function in the numerator when  $\omega \rightarrow 0$ . In addition, Figure 3a shows an apparent frequency gap in the low-frequency region. We will come back to this matter further down; for now, let

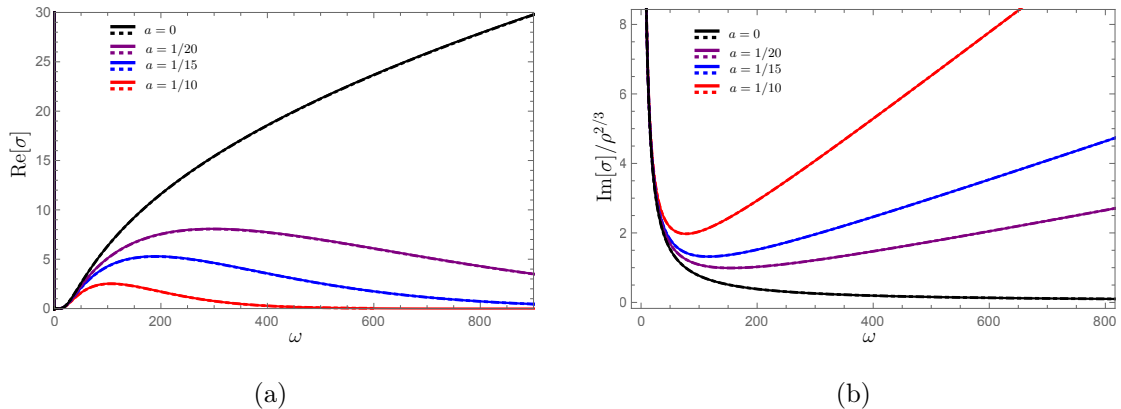


**Figure 3:** Portraits of the real (a) and imaginary (b) components of the conductivity as a function of the frequency. Again, our analytical computations (solid lines) show an excellent agreement with numerical ones (dashed lines). These plots were generated at  $T \approx 0.99994 T_c$  with  $\langle \mathcal{O} \rangle \approx 7.780$ , considering  $\ell = 1$  and  $r_h = 1$ .

us just denote the width of this gap as  $\omega_g$ . For frequencies beyond this gap,  $\omega > \omega_g$ , the function  $\omega^{1/2}$  dominates the behavior of  $\text{Re}[\sigma]$ , establishing a monotonically increasing asymptotic trend growing slower than the isotropic case sketched in Figure 2a.

When turning on the rotation ( $a \neq 0$ ), the asymptotic behavior of  $\text{Re}[\sigma]$  undergoes a significant transformation. In this scenario, the Dirac delta function at  $\omega = 0$  persists, accompanied by the emergence of a narrow gap at lower frequencies. This discernible gap can be defined by noting that the values assumed by the function  $\text{Re}[\sigma]$  within the interval  $0 < \omega \leq \omega_g$  are considerably smaller compared to those beyond this range,  $\omega > \omega_g$ . Consequently, within  $0 < \omega \leq \omega_g$ , we can effectively treat  $\text{Re}[\sigma]$  as zero. With this assumption, we can estimate the extent of the gap as a function of the rotation parameter, yielding

$$\omega_g = e^{-(\pi a/2\ell)} \left[ \frac{18}{5} \left(\frac{a}{\ell}\right)^4 - \frac{1167}{100} \left(\frac{a}{\ell}\right)^3 + \frac{67}{4} \left(\frac{a}{\ell}\right)^2 + 8 \left(\frac{a}{\ell}\right) + 6 \right], \quad (4.17)$$

wherein we observe a reduction of the gap driven by increasing the rotation. Also, this equation shows that the gap persists even in the absence of rotation, as expected from our earlier discussion. It is interesting to notice that, when  $\omega > \omega_g$ , and for a specific nontrivial value of  $a$ , the curve exhibits a peak, beyond which it undergoes an exponential fall. In this domain, at sufficiently high frequencies, the term  $a^2\omega/4\ell\Xi$  dominates with respect to  $\langle \mathcal{O} \rangle / \ell\omega$  contained in  $g(\omega, a)$ , giving rise to an asymptotic behavior of the form  $\text{Re}[\sigma] \sim \omega^2 \exp(-2\pi a^2\omega/4\ell\Xi)$ , which is now characterized by containing a proper dependence on the rotation parameter. Therefore, the combined effect of rotation and anisotropy in the background is accountable for inducing the peak and vanishing exponential behavior. This is a noteworthy characteristic in our model, as it resembles the behavior observed in field theory superconductor models as well with experiments, see for instance: [35–39].

On the other hand, regarding the imaginary part  $\text{Im}[\sigma]$ , the functional dependence on

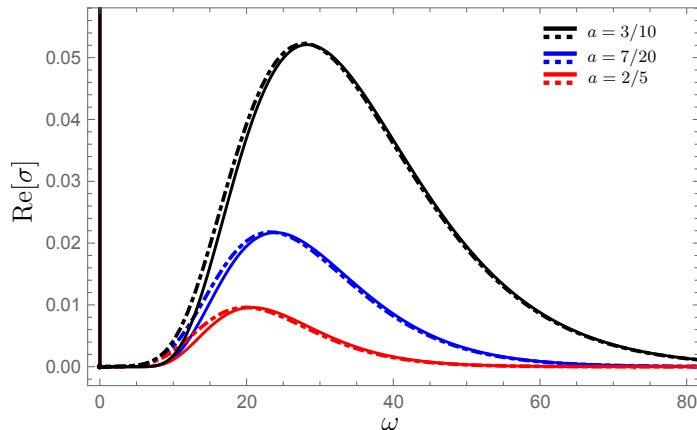


**Figure 4:** Illustration of the shift in  $\text{Re}[\sigma]$  for different values of the rotation parameter. The analytical curves are shifted to the right (solid) with respect to the numerical ones (dashed) as the rotation parameter adopts higher values. For this plot, we choose  $T \approx 0.99994 T_c$  for which  $\langle \mathcal{O} \rangle \approx 7.780$ , with parameters  $\ell = 1$  and  $r_h = 1$ .

the frequency is simpler as it is defined by the function  $\mathcal{G}(a, \omega)$  in 4.15b. The low-frequency behavior is given by  $\text{Im}[\sigma] \sim 1/\omega$ , while there is a minimum above which the behavior follows a linear trend,  $\text{Im}[\sigma] \sim \omega$ . This holds even in the scenario without rotation. Nonetheless, as seen in Figure 3b, notable distinctions emerge: in the scenario devoid of rotation  $a = 0$ , the minimum is located at a significantly higher frequency compared to cases with nontrivial rotation. Additionally, the slope of the dominant linear function at high frequencies is smaller, leading to a slower-growing behavior. To end this section, let us remark that our analytical findings (solid lines) show strong correspondence with the numeric (dashed lines) as occurred in the previous scenario. Nevertheless, regarding  $\text{Re}[\sigma]$ , the correspondence is sufficiently good only when the rotation parameter is small, for example within the interval  $0 \leq a \leq 1/4$ . For higher values of the rotation parameter, the analytical curves of  $\text{Re}[\sigma]$  shift to the right compared to the numerical ones, see Figure 4.

## 5 Turning on a uniform external magnetic field

This section is devoted to studying the transformation of the vortex lattice induced by an external magnetic field in our holographic superconductor. In doing so, we offer a comprehensive derivation and revision of fundamental aspects concerning the introduction of a uniform external magnetic field and the construction of the vortex lattice model formerly presented in [1]. To maintain a clear contrast with earlier work, we will adhere to the notation introduced in [1] throughout subsequent sections. Additionally, as a novel application of this theoretical framework, we successfully replicate the experimental observations of a LiFeAs superconductor.

Type II superconductors are characterized by two critical magnetic fields: the lower one,  $B_{c1}$ , and the upper one,  $B_{c2}$ . Below  $B_{c1}$ , perfect diamagnetism is observed. Beyond

this threshold, vorticity emerges when the external magnetic field exceeds  $B > B_{c1}$ , and the formation of a vortex lattice becomes favorable as the field approaches the upper critical value,  $B_{c2}$ , from below.

The emergence of the vortex lattice stems from the minimization of the free energy at magnetic field magnitudes below the upper critical value,  $B_{c2}$ , as initially observed in [20]. This approach involves inducing the condensation of the scalar field  $\Psi$  by varying the external magnetic field perpendicular to the Lifshitz boundary ( $u = 0$ ) while keeping the temperature and chemical potential constant. To address this phenomenon, we must solve the system of equations (2.6) in the vicinity of the upper critical magnetic field, using a perturbation parameter,  $\epsilon = (B_{c2} - B)/B \ll 1$ . The series expansion of the fields for this purpose is as follows

$$\Psi(u, \vec{y}) = \epsilon^{1/2} \Psi_1(u, \vec{y}) + \epsilon^{3/2} \Psi_2(u, \vec{y}) + \dots, \quad (5.1a)$$

$$A_\mu(u, \vec{y}) = A_\mu^{(0)}(u, \vec{y}) + \epsilon A_\mu^{(1)}(u, \vec{y}) + \dots, \quad (5.1b)$$

Notice that the spacetime indices  $\mu = (t, \phi, x, y)$  run on the boundary coordinates.

In refining the ansatz, we can still impose desired physical conditions. In our case, we seek regularity and periodicity of the condensate, along with a constant magnetic field normal to the boundary and a constant chemical potential also at the boundary. In terms of the field components we implement these conditions as

$$\Psi_1(u, \vec{y}) = \Phi(u, y) e^{ipx}, \quad A_x^{(0)}(u, \vec{y}) = B y, \quad A_t^{(0)}(u, \vec{y}) = A_t^{(0)}(u), \quad A_\phi^{(0)}(u, \vec{y}) = A_\phi^{(0)}(u) \quad (5.2)$$

By replacing the expansions (5.1) in the field equations (2.9a)-(2.9e), we obtain the non-trivial zeroth-order Maxwell equations

$$A_t^{(0)''} - \left[ (\Xi^2 - 1) \frac{f'}{f} - \frac{2(z-1)\Xi^2 - z}{u} \right] A_t^{(0)'} - \frac{a\Xi}{\ell^2} \left[ \frac{f'}{f} - \frac{2(z-1)}{u} \right] A_\phi^{(0)'} = 0, \quad (5.3a)$$

$$A_\phi^{(0)''} + \left[ \Xi^2 \frac{f'}{f} - \frac{2(z-1)\Xi^2 + 2 - z}{u} \right] A_\phi^{(0)'} + a\Xi \left[ \frac{f'}{f} - \frac{2(z-1)}{u} \right] A_t^{(0)'} = 0, \quad (5.3b)$$

The rest of the equations straightforwardly yield  $A_y^{(0)}(u, \vec{y}) = 0$ . Notice that there is no mixing between the scalar and the Maxwell fields at this order, facilitating the analytical solution

$$A_t^{(0)}(u) = \mu - \rho \left( \frac{u}{r_h} \right)^{3-z}, \quad A_\phi^{(0)}(u) = \nu - \zeta \left( \frac{u}{r_h} \right)^{3-z}, \quad (5.4)$$

with  $\zeta = -\frac{a}{\Xi} \rho$ . Regular boundary conditions—both asymptotically and at the horizon—constrain the parameters in the following manner: the critical exponent must lie within the interval  $1 \leq z < 3$ , while the constants are fixed as  $\rho = r_h^{3-z} \mu$  and  $\zeta = r_h^{3-z} \nu$ .

On the other hand, the zeroth-order scalar equation associated with (2.8) is

$$\begin{aligned} & \left[ u^{z+2} \partial_u \left( \frac{f}{u^{z+2}} \partial_u \right) + \left( \frac{\ell u}{r_h} \right)^{2(z-1)} \frac{(\ell^2 \Xi A_t^{(0)} + a A_\phi^{(0)})^2}{r_h^2 f} - \ell^2 \left( \frac{m^2}{u^2} + \frac{(a A_t^{(0)} + \Xi A_\phi^{(0)})^2}{r_h^2} \right) \right] \Phi \\ & = \left( \frac{\ell^2}{r_h} \right)^2 \left[ -\partial_{yy}^2 + (By - p)^2 \right] \Phi. \end{aligned} \quad (5.5)$$

One can show that the product separable ansatz  $\Phi(u, y) = R_n(u) \gamma_n(y; p)$  leads to two integrable differential equations. In fact, it is widely known that one of the equations results in a one-dimensional Schrödinger-like equation

$$\left( -\partial_{YY}^2 + \frac{Y^2}{4} \right) \gamma_n(y; p) = \frac{\lambda_n}{2} \gamma_n(y; p), \quad (5.6)$$

where the auxiliary variable  $Y := \sqrt{2B}(y - p/B)$  was introduced. Equation (5.6) dictates the spatial transversal distribution of the order parameter and its solution is determined in terms of the Hermite polynomials as follows

$$\gamma_n(y; p) = e^{-Y^2/4} H_n(Y), \quad (5.7)$$

together with the restriction on the eigenvalues  $\lambda_n = 2n + 1$ , with  $n \in \mathbb{Z}_{\geq 0}$ .

The remaining piece to be determined is often referred to as the radial part of  $\Phi$ . The corresponding radial equation takes the form

$$\begin{aligned} R_n''(u) + \left( \frac{f'}{f} - \frac{z+2}{u} \right) R_n'(u) = & \left[ - \left( \frac{\ell u}{r_h} \right)^{2(z-1)} \frac{(\ell^2 \Xi A_t^{(0)} + a A_\phi^{(0)})^2}{r_h^2 f^2} \right. \\ & \left. + \frac{\ell^2}{f} \left( \frac{m^2}{u^2} + \frac{(a A_t^{(0)} + \Xi A_\phi^{(0)})^2}{r_h^2} \right) + \left( \frac{\ell^2}{r_h} \right)^2 \frac{B \lambda_n}{f} \right] R_n(u). \end{aligned} \quad (5.8)$$

This equation describes the superconducting phase transition, and its solution requires a more detailed elaboration, which will be provided in the next section.

## 5.1 The external magnetic field

Upon a brief inspection of Eq. (5.8), it becomes evident that the external magnetic field plays a significant role in the dynamics of the radial mode. As we proceed to delve into this issue, the consistency of the solution unveils a relationship between the upper critical magnetic field and the black hole parameters.

The standard holographic prescription provides the renormalizable boundary form of the scalar field as given below

$$R(u) = J_- u^{\Delta_-} + J_+ u^{\Delta_+}, \quad (5.9)$$

where the scaling dimensions are  $\Delta_\pm = \frac{z+3 \pm \sqrt{(z+3)^2 + 4\ell^2 m^2}}{2}$ . Without loss of generality, we may impose the boundary condition  $J_- = 0$ , and  $J_+ = J$  with scaling dimension  $\Delta_+ = \Delta$ .



Similarly, we propose a near-horizon Taylor expansion of  $R(u)$  around  $u = 1$ , namely

$$R(u) = R(1) + R'(1)(u - 1) + \frac{1}{2}R''(1)(u - 1)^2 + \dots \quad (5.10)$$

Evaluation of Eq. (5.8) permits to algebraically solve order by order the coefficients of the series in terms of  $R(1)$

$$R'(1) = -\frac{\ell^2(m^2 r_h^2 + \ell^2 B)}{r_h^2(z+3)} R(1), \quad (5.11a)$$

$$R''(1) = \frac{1}{2(z+3)^2} \left\{ -\left(\frac{\ell}{\Xi}\right)^2 \left(\frac{\ell}{r_h}\right)^{2z} [A_t^{(0)'}(1)]^2 + \ell^2 m^2 [\ell^2 m^2 + 2(z+3)] \right. \\ \left. + \frac{\ell^4 B}{r_h^2} \left[2\ell^2 m^2 + \frac{\ell^4 B}{r_h^2}\right] \right\} R(1). \quad (5.11b)$$

Once again, the matching method described in [28] becomes relevant. Ensuring continuity and regularity requires a smooth matching between (5.9) and (5.10), and their derivatives, within a specific region of the bulk domain, say  $u = u_m$ . This matching can be achieved at the expense of the following algebraic constraints

$$J u_m^\Delta = \frac{r_h^2(z+3) + \ell^2(m^2 r_h^2 + \ell^2 B)}{r_h^2(z+3)} R(1) - \frac{\ell^2(m^2 r_h^2 + \ell^2 B)}{r_h^2(z+3)} R(1) u_m + \frac{1}{4(z+3)^2} \\ \times \left\{ \ell^2 m^2 [\ell^2 m^2 + 2(z+3)] + \frac{\ell^4 B}{r_h^2} \left[2\ell^2 m^2 + \frac{\ell^4 B}{r_h^2}\right] - \left(\frac{\ell}{\Xi}\right)^2 \left(\frac{\ell}{r_h}\right)^{2z} [A_t^{(0)'}(1)]^2 \right\} \\ \times R(1)(u_m - 1)^2, \quad (5.12a)$$

$$J \Delta u_m^{\Delta-1} = -\frac{\ell^2(m^2 r_h^2 + \ell^2 B)}{r_h^2(z+3)} R(1) + \frac{1}{2(z+3)^2} \left\{ -\left(\frac{\ell}{\Xi}\right)^2 \left(\frac{\ell}{r_h}\right)^{2z} [A_t^{(0)'}(1)]^2 + \ell^2 m^2 [\ell^2 m^2 \right. \\ \left. + 2(z+3)] + \frac{\ell^4 B}{r_h^2} \left[2\ell^2 m^2 + \frac{\ell^4 B}{r_h^2}\right] \right\} R(1)(u_m - 1). \quad (5.12b)$$

A most relevant implication arises from the evaluation of (5.12) at the upper critical magnetic field,  $B \approx B_{c2}$ , consistent with the perturbation parameter  $\epsilon \ll 1$ , and the subsequent insertion of the expression for  $A_t^{(0)'}(1) = (z-3) \frac{\rho}{r_h^{3-z}}$  obtained from (5.4). We are left with a consistency condition which can be read as a formula for the upper critical magnetic field in terms of the critical temperature, i.e.,

$$B_{c2} = \left(\frac{\ell^{z+1} \Xi}{z+3}\right)^{2/z} \frac{T^{2/z}}{\ell^4 \eta} \left\{ -\delta + \left[ \chi + (\delta^2 - \chi) \left(\frac{T_c}{T}\right)^{6/z} \right]^{1/2} \right\}, \quad (5.13)$$

where the constants

$$\eta = (1 - u_m) [(2 - \Delta) u_m + \Delta], \quad (5.14a)$$

$$\chi = 2(z+3) (2(z+3) u_m^2 - \ell^2 m^2 \eta^2), \quad (5.14b)$$

$$\delta = 2u_m [(z+3) + \ell^2 m^2 (1 - u_m)] + \Delta (1 - u_m) [2(z+3) + \ell^2 m^2 (1 - u_m)], \quad (5.14c)$$

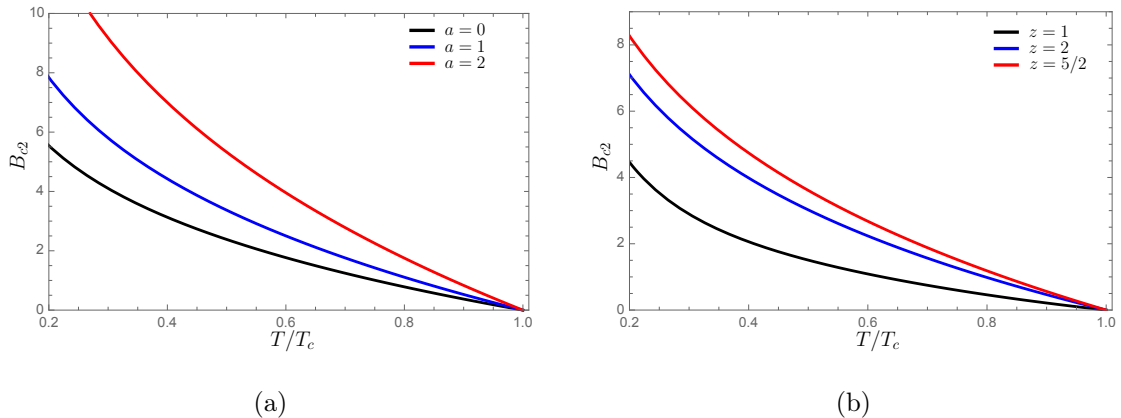


**Figure 5:** Figure (a) shows the behavior of the upper critical magnetic field by setting  $\ell^2 m^2 = -3$ ,  $u_m = 0.8$ , and  $z = 2$  while taking diverse values of the rotation parameter. On the other hand, Figure (b) is obtained by setting  $\ell^2 m^2 = -3$ ,  $u_m = 0.9$  and  $a = 1$  while considering different values of the critical exponent  $z$ .

introduce alleviated notation. The critical temperature is given by

$$T_c = \frac{z+3}{\ell^{z+1}\Xi} \frac{1}{(\delta^2 - \chi)^{z/6}} \left[ \eta^2 \ell^{2z} (z-3)^2 \left( \frac{\ell}{\Xi} \right)^2 \rho^2 \right]^{z/6}. \quad (5.15)$$

A quick check-up reveals that  $B_{c2}$  goes as predicted by the Ginzburg-Landau theory near the critical temperature, with  $B_{c2} \propto (1 - T/T_c)$ . This behavior is depicted in Figures 5a and 5b.

## 5.2 The vortex configuration

As previously anticipated, our focus lies in developing a model for the vortex lattice deformation in measurable superconductors. At this stage, we can conclude the theory we have formulated and proceed to characterize the lattice properties, similar to the investigations carried out in previous works [1, 20, 40].

Our construction is founded upon the most stable modes of the scalar field, which are the lowest (zero) orders, as illustrated in [20]. The transversal part contributes then with

$$\gamma_0(y; p_k) = \exp \left[ -\frac{1}{2r_0^2} (y - p_k r_0^2)^2 \right], \quad (5.16)$$

where  $r_0 = 1/\sqrt{B}$ . The full lattice, however, requires a linear superposition over all the  $p_k$  parameters

$$\Psi_1(u, \vec{y}) = R_0(u) \gamma_L(\vec{y}), \quad \text{with} \quad \gamma_L(\vec{y}) := \sum_{k=-\infty}^{\infty} c_k e^{ip_k x} \gamma_0(y; p_k). \quad (5.17)$$

Similarly,  $R_0(u)$  stands for the lowest order solution to the radial equation (5.8).

The lattice is characterized by the periodic occurrence of fundamental cells. However, notice from (5.17) that this function is already periodic along the  $x$  direction, but not necessarily along the  $y$  direction. Full periodicity can be introduced by means of the reparametrization

$$c_k \equiv e^{iq_k}, \quad q_k \equiv \alpha k^2, \quad p_k \equiv \beta k, \quad (5.18)$$

in terms of the arbitrary constants  $\alpha$  and  $\beta$ . Using this definition, we can express  $\gamma_L$  in terms of the elliptic theta function  $\vartheta_3$  as follows

$$\gamma_L(\vec{y}) = e^{-y^2/2r_0^2} \vartheta_3(v, \tau). \quad (5.19)$$

Above, new convenient coordinate and parameter were introduced

$$v := \frac{\beta}{2\pi}(x - iy), \quad \tau := \frac{1}{2\pi}(2\alpha + i\beta^2 r_0^2). \quad (5.20)$$

The  $\gamma_L$  function inherits the symmetry properties of  $\vartheta_3$ . It is thus not difficult to show that  $\gamma_L$  exhibits pseudo-periodicity in the directions characterized by the vectors

$$\vec{b}_1 = \frac{2\pi}{\beta} \partial_x, \quad (5.21a)$$

$$\vec{b}_2 = \frac{2\alpha}{\beta} \partial_x - \beta r_0^2 \partial_y. \quad (5.21b)$$

Accordingly, the explicit transformations manifesting the aforementioned pseudo-periodicity are

$$\gamma_L\left(x + \frac{2\pi}{\beta}, y\right) = \gamma_L(x, y), \quad (5.22a)$$

$$\gamma_L\left(x + \frac{2\alpha}{\beta}, y - \beta r_0^2\right) = \exp[-i(\alpha + \beta x)] \gamma_L(x, y). \quad (5.22b)$$

The lattice structure is fully attained up to this point. It is straightforward to verify that the modulus squared  $|\gamma_L|^2$  is already periodic while fundamental regions conforming the lattice are generated by the vectors (5.21). Consequently, any point on the lattice can be expressed as a linear combination of  $\vec{b}_1$  and  $\vec{b}_2$ . In agreement with Ginzburg-Landau theory, here the magnetic flux is quantized as  $B \times 2\pi r_0^2 = 2\pi$ .

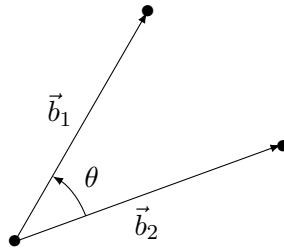


**Figure 6:** Fundamental vectors of the vortex lattice associated with the type-II holographic superconductor.

The zeros of  $|\gamma_L|$  indicate the locations of vortex cores, where the order parameter vanishes ( $\langle \mathcal{O} \rangle \sim |\gamma_L| = 0$ ). These zeros can be expressed in a compact form as given in the following equation [20]

$$\vec{x}_{n_1, n_2} = \left(n_1 + \frac{1}{2}\right) \vec{b}_1 + \left(n_2 + \frac{1}{2}\right) \vec{b}_2, \quad (5.23)$$

for integers  $n_1$  and  $n_2$ . Now, using equations (5.21) and (5.23), we can establish the following relationships between two adjacent vectors of equal magnitude in the fundamental cell

$$\cos \theta = \sqrt{1 - \frac{\beta^4}{4\pi^2 B^2}}, \quad \alpha = \pi \cos \theta, \quad (5.24)$$

wherein the angle between adjacent vectors is denoted by  $\theta$ , as shown in Figure 6. In this manner, relations (5.24) provide a mechanism for continuously deforming the lattice structure by virtue of the external magnetic field. It is noteworthy that the parameter  $\beta$  remains arbitrary and can be appropriately chosen as a function of the external magnetic field. Specifically, we can select  $\beta$  in such a way that the vortex lattice deforms in a desired manner as the external magnetic field is applied. The specific function that relates  $\beta$  to the magnetic field is expected to depend on the properties of the material as elaborated in the following discussion on an experimental realization.

### Vortex lattice deformation of a lithium-iron-arsenide (LiFeAs) superconductor

As we already remarked, the relations (5.24) define continuous deformations of a given vortex lattice driven by the external magnetic field. Here we want to study how these deformations take place when starting from a particular vortex configuration. In particular, we would like to go beyond the theoretical scopes of the model presented here and qualitatively describe some experimental behavior concerning the vortex lattice transformation of iron-based superconductors. We recall that the description of a FeSe compound was recently detailed in [1].

An interesting iron-based superconductor showing experimental vortex lattice transformations is the LiFeAs superconductor explored in [41]. Unlike the FeSe case, here the transformation occurs in a slightly different regime of the external magnetic field but evolving in the same direction, from a triangular to a square lattice. Concretely, the transformation occurs from a triangular lattice at 2 T, passing through intermediate configurations at 3 T, 3.5 T, and 3.75 T and ending with a square structure at 4 T. In order to model such a behavior, the  $\beta$  parameter must be considered linear in  $B$ , i.e.

$$\beta = a_1 + a_2 B, \quad 2 \text{ T} < B < 4 \text{ T}, \quad (5.25)$$

with coefficients  $a_1 = 1.57161 \text{ T}^{1/2}$  and  $a_2 = 0.85991 \text{ T}^{-1/2}$ , while it is important to bear in mind that the temperature is kept fixed in the experiment. The behavior reproduced by our holographic model is illustrated in Figure 7.

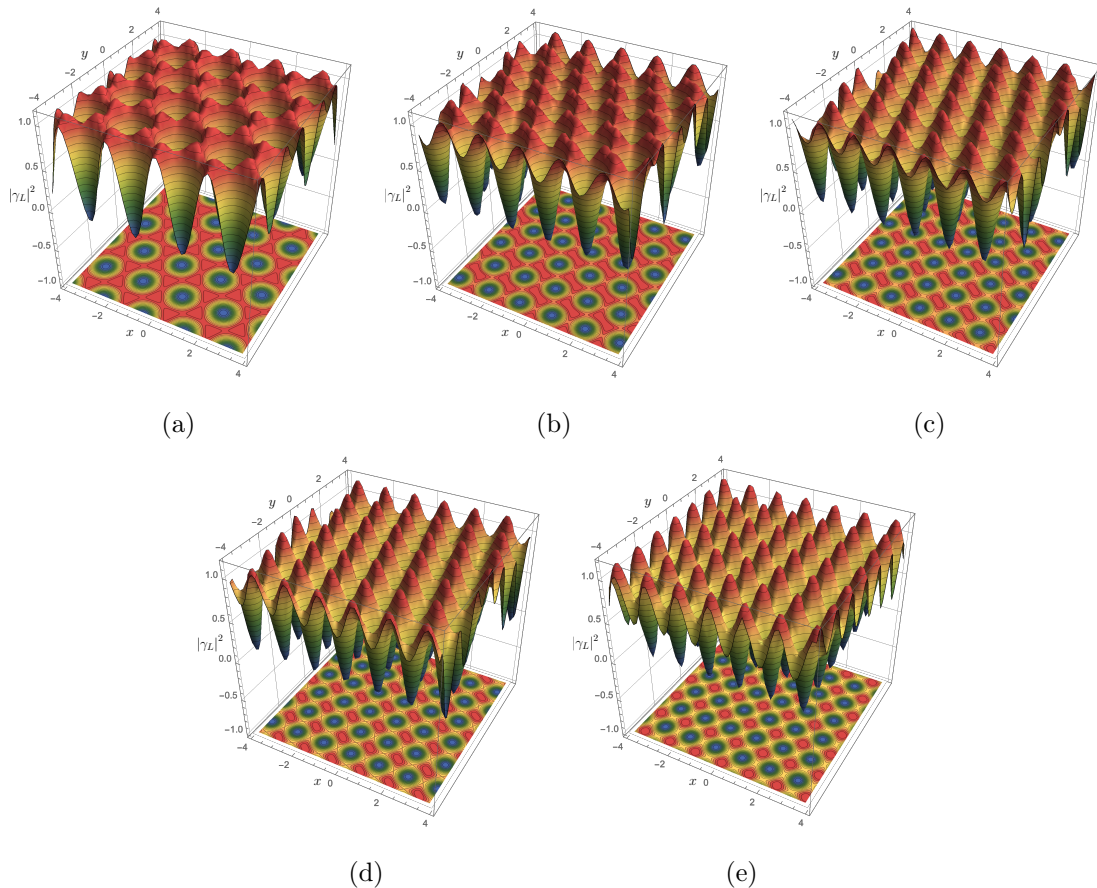


**Figure 7:** The transformation of the LiFeAs superconductor vortex lattice from the triangular (a) at 2 T, passing the intermediate states (b)-(d) at 3, 3.5, and 3.75 T respectively, to the square lattice (e) at 4 T, when increasing external magnetic field.

## 6 Conclusions and discussion

We have developed a holographic model for a type-II s-wave superconductor that incorporates rotating and anisotropic aspects in the black hole background. Using both analytical and numerical approaches, we examined how rotation and anisotropy influence the properties of the superconductor model. Concerning the condensation phenomena, our findings reveal that an increment (or decrement) in the rotation leads to a corresponding reduction (or increment) in the magnitude of the condensation curve, as illustrated in Figure 1. This scaling effect was qualitatively reproduced by the analytical approach, in which the matching method was used, and supported by the numerical approach using the shooting method. Regarding the results for the AC conductivity, we worked out two cases, the isotropic ( $z = 1$ ,  $\Delta = 1$ ) and the anisotropic one ( $z = 2$ ,  $\Delta = 1$ ), where novel closed formulas for the conductivity were obtained. The isotropic case remained unaffected by the presence of a nontrivial rotation, indicating that to study the effect induced by this quantity, we must consider the anisotropy of the background. In this regard, the interplay

between rotation and anisotropy brought forth a noteworthy behavior not reported in previous holographic models. Concretely, our results have shown that the rotation induces a peak in the low-frequency region of  $\text{Re}[\sigma]$ , followed by an exponentially vanishing tendency at higher frequencies. Moreover, our findings also revealed that the magnitude of the peak falls monotonically and is shifted to a lower frequency as the rotation increases, see Figure 3a. Altogether, this behavior aligns with predictions from high-temperature superconductor models and experiments [35–39]. Within this context, the appearance of the peak and the vanishing behavior at high frequencies are attributed to the effects of quasiparticle damping driven by impurities or defects in the superconducting system. Consequently, our results suggest an interesting connection between the rotation of the anisotropic black hole in our holographic superconductor model and quasiparticle damping in superconducting materials. In relation to the imaginary component  $\text{Im}[\sigma]$ , the effect of the rotation is manifested in increasing the amplitude of the curve at higher frequencies as the rotation parameter increases, see Figure 3b.

Furthermore, we considered the superconducting system subject to a uniform magnetic field. We employed the matching method to derive an analytical expression for the upper critical magnetic field, the threshold below which the vortex phenomenon occurs. The results revealed how this upper critical magnetic field gets affected by the dynamical scaling exponent  $z$  and the rotation of the background  $a$ . In both cases, the effect is no more than re-scaling the upper critical magnetic field, as illustrated in Figure 5.

To construct the Abrikosov vortex lattice, we adopted an approach inspired on previous works [1, 20, 40]. Our method yielded promising results as we were able to describe continuous transformations of the vortex lattice driven by the external magnetic field in a unified manner. Notice that such transitions can also be described in field theory superconductivity by modifications of the Ginzburg-Landau theory, although diverse lattice transformations arise depending on the materials and the experimental setups [42–44]. Specifically, by appropriately choosing the  $\beta$  parameter as a function of the external magnetic field, we successfully reproduced the vortex transformation observed in recent experiments concerning iron-based superconductors, concretely LiFeAs [41]. In this case, it was sufficient to adjust the  $\beta$  parameter as a linear function of the external magnetic field  $B$ , suggesting that the  $\beta$  parameter will be defined according to the properties of the superconducting material under consideration. The freedom in choosing  $\beta$  offers additional modeling possibilities that are worth investigating in detail for their potential application to other relevant findings.

As a final comment, we would like to draw attention to a noteworthy point of comparison with our model that was presented in [45]. Therein, the authors introduce a numerical approach for the construction of the vortex lattice capable of reproducing triangular and square structures driven by both temperature and the external magnetic field. It will be interesting to include the effect of both temperature and magnetic field within our analytic approach. The first idea that comes to mind consists in assuming a more general dependence of the angle between the fundamental vectors on the external magnetic field and the temperature,  $\theta = \theta(B, T)$ . This relation can be realized by making the parameter  $\beta$  dependent on the temperature as well (think of the coefficients  $a_1$  and  $a_2$  depending on  $T$ ,

for instance). Thus, we arrive at the need to perform a series of experiments in which the vortex lattice deformation is driven by changes in both the temperature and the magnitude of the external magnetic field. The corresponding experimental data would allow us to fit the observed  $\theta = \theta(B, T)$  dependence.

## Acknowledgments

All the authors are grateful to Manuel de la Cruz for enriching discussions. The authors acknowledge financial support from FORDECYT-PRONACESCONACYT Grant No. CF-MG-2558591, CONAHCYT Grant No. A1-S-38041, and VIEP-BUAP Grant. JAHM also acknowledges support from CONAHCYT through a PhD Grant No. 750974. DFHB and JAMZ are also grateful to CONAHCYT for a *Estancias posdoctorales por México* Grant No. 372516 and project 898686, respectively.

## References

- [1] J.A. Herrera-Mendoza, D.F. Higuera-Borja, J.A. Méndez-Zavaleta, A. Herrera-Aguilar and F. Pérez-Rodríguez, *Vortex structure deformation of rotating Lifshitz holographic superconductors*, *Phys. Rev. D* **106** (2022) L081902 [[2208.05988](#)].
- [2] J.M. Maldacena, *The Large N limit of superconformal field theories and supergravity*, *Adv. Theor. Math. Phys.* **2** (1998) 231 [[hep-th/9711200](#)].
- [3] S.A. Hartnoll, C.P. Herzog and G.T. Horowitz, *Building a Holographic Superconductor*, *Phys. Rev. Lett.* **101** (2008) 031601 [[0803.3295](#)].
- [4] C.P. Herzog, P.K. Kovtun and D.T. Son, *Holographic model of superfluidity*, *Phys. Rev. D* **79** (2009) 066002 [[0809.4870](#)].
- [5] M. Taylor, *Non-relativistic holography*, [0812.0530](#).
- [6] E. Ayon-Beato, A. Garbarz, G. Giribet and M. Hassaine, *Lifshitz Black Hole in Three Dimensions*, *Phys. Rev. D* **80** (2009) 104029 [[0909.1347](#)].
- [7] E. Ayon-Beato, A. Garbarz, G. Giribet and M. Hassaine, *Analytic Lifshitz black holes in higher dimensions*, *JHEP* **04** (2010) 030 [[1001.2361](#)].
- [8] E. Ayón-Beato, M. Bravo-Gaete, F. Correa, M. Hassaine and M.M. Juárez-Aubry, *Microscopic entropy of higher-dimensional nonminimally dressed Lifshitz black holes*, *Phys. Rev. D* **100** (2019) 044024 [[1904.09391](#)].
- [9] M. Bravo-Gaete and M.M. Juárez-Aubry, *Thermodynamics and Cardy-like formula for nonminimally dressed, charged Lifshitz black holes in new massive gravity*, *Class. Quant. Grav.* **37** (2020) 075016 [[2002.10520](#)].
- [10] M. Bravo-Gaete, M.M. Juárez-Aubry and G. Velazquez-Rodriguez, *Lifshitz black holes in four-dimensional critical gravity*, *Phys. Rev. D* **105** (2022) 084009 [[2112.01483](#)].
- [11] S. Kachru, X. Liu and M. Mulligan, *Gravity duals of Lifshitz-like fixed points*, *Phys. Rev. D* **78** (2008) 106005 [[0808.1725](#)].
- [12] S.A. Hartnoll, C.P. Herzog and G.T. Horowitz, *Holographic Superconductors*, *JHEP* **12** (2008) 015 [[0810.1563](#)].

- [13] S.A. Hartnoll, *Lectures on holographic methods for condensed matter physics*, *Class. Quant. Grav.* **26** (2009) 224002 [[0903.3246](#)].
- [14] S. Gangopadhyay and D. Roychowdhury, *Analytic study of properties of holographic superconductors in Born-Infeld electrodynamics*, *JHEP* **05** (2012) 002 [[1201.6520](#)].
- [15] S. Gangopadhyay and D. Roychowdhury, *Analytic study of Gauss-Bonnet holographic superconductors in Born-Infeld electrodynamics*, *JHEP* **05** (2012) 156 [[1204.0673](#)].
- [16] E. Nakano and W.-Y. Wen, *Critical magnetic field in a holographic superconductor*, *Phys. Rev. D* **78** (2008) 046004 [[0804.3180](#)].
- [17] T. Albash and C.V. Johnson, *A Holographic Superconductor in an External Magnetic Field*, *JHEP* **09** (2008) 121 [[0804.3466](#)].
- [18] T. Albash and C.V. Johnson, *Vortex and Droplet Engineering in Holographic Superconductors*, *Phys. Rev. D* **80** (2009) 126009 [[0906.1795](#)].
- [19] T. Albash and C.V. Johnson, *Phases of Holographic Superconductors in an External Magnetic Field*, [0906.0519](#).
- [20] K. Maeda, M. Natsuume and T. Okamura, *Vortex lattice for a holographic superconductor*, *Phys. Rev. D* **81** (2010) 026002 [[0910.4475](#)].
- [21] M. Montull, A. Pomarol and P.J. Silva, *The Holographic Superconductor Vortex*, *Phys. Rev. Lett.* **103** (2009) 091601 [[0906.2396](#)].
- [22] A. Adams, P.M. Chesler and H. Liu, *Holographic Vortex Liquids and Superfluid Turbulence*, *Science* **341** (2013) 368 [[1212.0281](#)].
- [23] C.-Y. Xia, H.-B. Zeng, H.-Q. Zhang, Z.-Y. Nie, Y. Tian and X. Li, *Vortex Lattice in a Rotating Holographic Superfluid*, *Phys. Rev. D* **100** (2019) 061901 [[1904.10925](#)].
- [24] A. Srivastav and S. Gangopadhyay, *Vortices in a rotating holographic superfluid with Lifshitz scaling*, *Phys. Rev. D* **107** (2023) 086005 [[2302.01030](#)].
- [25] Y. Bu, *Holographic superconductors with  $z = 2$  Lifshitz scaling*, *Phys. Rev. D* **86** (2012) 046007 [[1211.0037](#)].
- [26] J.-W. Lu, Y.-B. Wu, P. Qian, Y.-Y. Zhao and X. Zhang, *Lifshitz Scaling Effects on Holographic Superconductors*, *Nucl. Phys. B* **887** (2014) 112 [[1311.2699](#)].
- [27] M. Natsuume and T. Okamura, *Holographic Lifshitz superconductors: Analytic solution*, *Phys. Rev. D* **97** (2018) 066016 [[1801.03154](#)].
- [28] Z. Zhao, Q. Pan and J. Jing, *Notes on analytical study of holographic superconductors with Lifshitz scaling in external magnetic field*, *Phys. Lett. B* **735** (2014) 438 [[1311.6260](#)].
- [29] J. Sonner, *A Rotating Holographic Superconductor*, *Phys. Rev. D* **80** (2009) 084031 [[0903.0627](#)].
- [30] K. Lin and E. Abdalla, *Holographic Superconductors in a Rotating Spacetime*, *Eur. Phys. J. C* **74** (2014) 3144 [[1403.7407](#)].
- [31] A. Srivastav and S. Gangopadhyay, *Analytic investigation of rotating holographic superconductors*, *Eur. Phys. J. C* **79** (2019) 340 [[1902.01628](#)].
- [32] A. Herrera-Aguilar, J.A. Herrera-Mendoza and D.F. Higueta-Borja, *Rotating Spacetimes generalizing Lifshitz Black Holes*, *Eur. Phys. J. C* (2021) 874 [[2104.14514](#)].



- [33] G.T. Horowitz and M.M. Roberts, *Zero Temperature Limit of Holographic Superconductors*, *JHEP* **11** (2009) 015 [[0908.3677](#)].
- [34] G.T. Horowitz, *Introduction to Holographic Superconductors*, *Lect. Notes Phys.* **828** (2011) 313 [[1002.1722](#)].
- [35] W. Zimmermann, E. Brandt, M. Bauer, E. Seider and L. Genzel, *Optical conductivity of BCS superconductors with arbitrary purity*, *Physica C: Superconductivity* **183** (1991) 99.
- [36] F. Gao, G.L. Carr, C.D. Porter, D.B. Tanner, G.P. Williams, C.J. Hirschmugl et al., *Quasiparticle damping and the coherence peak in  $\text{YBa}_2\text{Cu}_3\text{O}_{7-\delta}$* , *Phys. Rev. B* **54** (1996) 700.
- [37] M. Dressel, *Electrodynamics of metallic superconductors*, *Advances in Condensed Matter Physics* **2013** (2013) 104379.
- [38] B. Michon, C. Berthod, C.W. Rischau, A. Ataei, L. Chen, S. Komiya et al., *Reconciling scaling of the optical conductivity of cuprate superconductors with planckian resistivity and specific heat*, *Nature Communications* **14** (2023) 3033.
- [39] R. Boyack, S. Mirabi and F. Marsiglio, *Electrical conductivity and nuclear magnetic resonance relaxation rate of eliashberg superconductors in the weak-coupling limit*, *Communications Physics* **6** (2023) 54.
- [40] H. Guo, F.-W. Shu, J.-H. Chen, H. Li and Z. Yu, *A holographic model of d-wave superconductor vortices with Lifshitz scaling*, *Int. J. Mod. Phys. D* **25** (2016) 1650021 [[1410.7020](#)].
- [41] S.S. Zhang, J.-X. Yin, G. Dai, H. Zheng, G. Chang, I. Belopolski et al., *Vector field controlled vortex lattice symmetry in  $\text{LiFeAs}$  using scanning tunneling microscopy*, *Phys. Rev. B* **99** (2019) 161103 [[1802.10059](#)].
- [42] Y. De Wilde, M. Iavarone, U. Welp, V. Metlushko, A.E. Koshelev, I. Aranson et al., *Scanning tunneling microscopy observation of a square abrikosov lattice in  $\text{LuNi}_2\text{B}_2\text{C}$* , *Phys. Rev. Lett.* **78** (1997) 4273.
- [43] V.G. Kogan, M. Bullock, B. Harmon, P. Miranovic-acute, L. Dobrosavljevic-acute Grujic-acute, P.L. Gammel et al., *Vortex lattice transitions in borocarbides*, *Phys. Rev. B* **55** (1997) R8693.
- [44] A.V. Putilov, C. Di Giorgio, V.L. Vadimov, D.J. Trainer, E.M. Lechner, J.L. Curtis et al., *Vortex-core properties and vortex-lattice transformation in  $\text{FeSe}$* , *Phys. Rev. B* **99** (2019) 144514.
- [45] C.-Y. Xia, H.-B. Zeng, Y. Tian, C.-M. Chen and J. Zaanen, *Holographic Abrikosov lattice: Vortex matter from black hole*, *Phys. Rev. D* **105** (2022) L021901 [[2111.07718](#)].